Analytica Chimica Acta 708 (2011) 44–51

Contents lists available at SciVerse ScienceDirect

Analytica Chimica Acta

journal homepage: www.elsevier.com/locate/aca

A sensitive enzymeless hydrogen-peroxide sensor based on epitaxially-grown Fe_3O_4 thin film

Jiang Yang[a], Hua Xiang[b], Li Shuai[a], Sundaram Gunasekaran[a,*]

[a] Department of Biological Systems Engineering, University of Wisconsin-Madison, 460 Henry Mall, Madison, WI 53706, USA
[b] Department of Materials Science and Engineering, University of Wisconsin-Madison, 1509 University Avenue, Madison, WI 53706, USA

ARTICLE INFO

Article history:
Received 20 July 2011
Received in revised form
27 September 2011
Accepted 30 September 2011
Available online 6 October 2011

Keywords:
Epitaxial
Fe_3O_4 film
Hydrogen peroxide
Electrochemical sensor

ABSTRACT

A novel and facile approach has been developed to synthesize thin films of magnetite (Fe_3O_4) with epitaxial needle-like columnar grains on titanium nitride (TiN) buffered substrate using DC magnetron reactive sputtering. TiN buffer layer was first sputtered onto a substrate at 550 °C as a preferable substrate for growth following sputtering of epitaxial crystalline Fe_3O_4 at 300 °C. The as-synthesized epitaxial Fe_3O_4 was extensively characterized. The electrocatalytic activity of the epitaxial Fe_3O_4 thin-film sensor against hydrogen peroxide (H_2O_2) reduction was rapid with a response time less than 5 s. The sensor also exhibited an acceptable stability, a satisfying sensitivity of 432.2 $\mu A\,mM^{-1}\,cm^{-2}$, good specificity to the substrate, a dynamic working range of up to 0.7 mM and a low detection limit of 1.0 μM. The sensor performance correlated well ($R^2 = 0.996$) with results obtained using a commercial HPLC-UV device. The sensor performance was robust and accurate in measuring H_2O_2 in some complex matrices. The advantages of relative simplicity and ease of mass production make the epitaxial Fe_3O_4 thin film promising candidate for use in sensing applications.

1. Introduction

Rapid, sensitive, and accurate determination of H_2O_2 has become a major concern not only because it is a by-product of several important oxidases, but also because it serves as a significant mediator in food, clinical, industrial, pharmaceutical, and environmental products [1]. Though widely used in applications such as aseptic packaging, antimicrobial wound treating, disinfecting, dental bleaching, food processing etc., H_2O_2 is not entirely safe. Industrial strength H_2O_2 is a strong oxidizer and is able to corrode eyes and skin, causing irreversible damage. H_2O_2 found in the eye lens and aqueous fluid, at concentrations only slightly higher than normal physiological levels, produced a significant number of DNA single-strand breaks in lens epithelial cell cultures [2] and tissue damage [3] including blindness. If consumed in excess, H_2O_2 can induce potentially life-threatening neurological reactions and damage to the upper gastrointestinal tract [4]. Health Canada and US Food and Drug Administration (FDA) have issued a warning in 2006 against human consumption of H_2O_2.

Current methods to detect H_2O_2 such as titrimetry, chemiluminescence, and spectrometry suffer from several shortcomings [5]. For instance, they are often laborious, time-consuming, lab-based, costly in devices or consumables such as enzymes, and require trained individuals to perform the test. Electrochemical approaches for detecting various analytes have received extensive attention in recent years due to their low cost, high sensitivity, fast response, accuracy, capability of operating in the presence of optically-interfering substances etc. [6]. Enzyme-based (i.e., horse radish peroxidase, HRP) [7] and enzymeless electrochemical H_2O_2 sensors [8] are very popular. However, there are intrinsic drawbacks of enzyme-based sensors such as complicated preparation steps, poor reproducibility, stringent operating conditions (pH, temperature, humidity, ionic strength etc.), high cost and most importantly unsuitablity for mass production [9,10], which limit their applications.

In contrast, enzymeless sensors are mostly based on metal, metal oxides or hybrid materials. Cao et al. synthesized Co_3O_4 nanoparticles and used them in H_2O_2 sensing [11]. Tian's group has successfully detected cellular H_2O_2 from living cancer cells based on ZnO nanosheets [12]. Chakraborty et al. used Pt nanoparticles in H_2O_2 electrochemical sensing [13]. A H_2O_2 sensor has also been fabricated using layer-by-layer assembled Fe_3O_4 nanoparticles and poly(diallyldimethylammonium chloride) (PDDA) through the electrostatic interaction [14]. Though good analytical performances have been achieved, these nanomaterial-based sensors are expensive and are difficult to mass produce for a wide range of applications. Therefore, developing simple, facile, and reliable enzymeless H_2O_2 sensors is a pressing need. Thin-film technology offers such advantages as low cost, simple synthesis, high durability, good electric properties, and possibility of mass manufacturing

* Corresponding author. Tel.: +1 608 262 1019; fax: +1 608 262 1228.
E-mail address: guna@wisc.edu (S. Gunasekaran).

0003-2670/$ – see front matter © 2011 Elsevier B.V. All rights reserved.
doi:10.1016/j.aca.2011.09.039

of high quality sensors [15]. For example, gold (Au) thin film as working electrodes for amperometric detection has already been commercialized and widely employed in high performance liquid chromatography (HPLC), microfluidics, and other techniques.

Herein, we report an approach to synthesize thin film of epitaxially-grown Fe_3O_4 with columnar grain structures in orientations of (0 0 1) on correspondingly-oriented TiN-buffered substrates by DC magnetron reactive sputtering and its usefulness in electrochemical H_2O_2 sensing. Fe_3O_4 is an artificial peroxidase mimetic with similar intrinsic activity to natural peroxidases but can hardly be inhibited or digested by proteases and other enzymes [16,17]. Fe_3O_4, the most stable iron oxide, is a ferromagnetic compound with inverse spinel structure and has been widely used as electrode materials with an electrical conductivity dramatically higher ($\times 10^6$ times) than that of ferric oxide (Fe_2O_3), resulting from fast electron exchange between Fe(II) and Fe(III). The as-developed enzyme-free electrochemical sensor based on epitaxially-grown crystalline Fe_3O_4 thin film (140-nm thick) we synthesized is simple, stable, rapid, highly sensitive for H_2O_2 sensing and suitable for mass production.

2. Materials and methods

2.1. Materials

D(+)-glucose, D(+)-maltose, β-D-lactose, L-ascorbic acid (AA), uric acid (UA), dopamine (DA), D-fructose, sucrose and mannose (from AlfaAesar); bovine serum albumin (BSA) (from Fisher Scientific); histamine, caffeine and casein (from Acros Organics); xanthan gum (from MP Biomedicals); and β-lactoglobulin (from Sigma–Aldrich) were purchased. All other reagents were of analytical grade and used without further purification. Food and medical samples for testing were purchased from local supermarket and they were centrifuged as needed. High quality deionized Milli-Q water (resistivity = 18.2 MΩ) was used throughout the experiments. N/Phos type Si wafer with (0 0 1) orientation and resistivity 1–20 Ω cm^{-1} (Wafer World Inc., FL, USA) was used as the substrate for material synthesis.

2.2. Instrumentation

X-ray diffraction (XRD) patterns were recorded using X'Pert RPO MRD high resolution diffractometer (PANalytical Inc., MA, USA) with Cu Kα radiation (λ = 0.15406 nm) at scanning rate of 4° min^{-1} and 2θ ranging from 30° to 90°. Surface morphology of the Si(0 0 1)/TiN/Fe_3O_4 was characterized by atomic force microscope (AFM) (Digital Instruments Inc., CA, USA). The magnetization hysteresis loops of the films were measured at room temperature by vibrating sample magnetometry (VSM) while the chemical states of Fe were confirmed by PHI 5400 x-ray photoelectron spectroscopy (XPS) (RBD Instruments Inc., OR, USA). Attenuated total reflectance-Fourier transform infrared spectroscopy (ATR-FTIR) was conducted with PerkinElmer Spectrum 100 (PerkinElmer, MA, USA). Chromatography analysis was performed using Dionex ICS-3000 HPLC system (Dionex Corporation, MA, USA) equipped with Supelcogel C-610H column at 30 °C and UV detector at 210 nm. Eluent was 0.1% phosphoric acid at a rate of 0.7 mL min^{-1} and H_2O_2 was eluted with a peak at about 13.8 min under these conditions.

All electrochemical measurements, including electrochemical impedance spectroscopy (EIS), were performed using a CHI 660D Electrochemical Analyzer (CH Instrument Inc., Austin, TX, USA). A conventional three-electrode configuration was used with Pt wire counter electrode, saturated Ag/AgCl (3 M KCl) reference electrode and Fe_3O_4 or TiN-buffered Si(0 0 1) electrodes as the working electrode. All potentials were referenced to the Ag/AgCl (3 M KCl) electrode. 100 mM KCl solution containing equimolar $[Fe(CN)_6]^{4-/3-}$ redox probes was used as supporting electrolyte for EIS with applied frequencies from 0.1 Hz to 100 kHz under open circuit potentials. Equivalent circuit and simulation data fitting were achieved using ZVIEW 2 software. All measurements were carried out at room temperature (25 ± 1 °C). Temperature control was monitored real-time by Traceable® Ultra™ thermometer from Fisher Scientific.

2.3. Preparation of epitaxially-grown Fe_3O_4 electrode

Si(0 0 1) substrate was cleaned using 3:1 of H_2SO_4:H_2O_2 for 10 min at 90 °C to remove any organic contaminants and subject to etch by 10% hydrogen fluoride (HF) solution for one minute to eliminate oxides on the surface. Synthesis of multi-layered stacks of substrate/TiN/Fe_3O_4 was conducted by DC magnetron reactive sputtering with a home-built system under base pressure better than 2.0×10^{-7} Torr, following recently reported procedures [18,19] with minor modifications. Briefly, 10-nm thick stoichiometric TiN buffer layer was first reactively sputtered on 3 mm × 3 mm Si(0 0 1) substrate (geometric area = 0.09 cm^2) in a mixed atmosphere of Ar and N_2 at the substrate temperature of 550 °C for 30 s at 250 W, which is required for epitaxial growth of Fe_3O_4 to eliminate any reactivity with Si substrate at high temperature. After cooling to room temperature, epitaxial crystalline Fe_3O_4 was deposited on the TiN layer under DC sputtering power of 60 W at 300 °C for 10 min under Ar and O_2. The deposition procedure was repeated once more to obtain a 140-nm-thick Fe_3O_4 thin film with epitaxial columnar grains. The substrate with Fe_3O_4 was fabricated as an electrode by connecting it to the surface of a glassy carbon electrode (GCE) with Flash-Dry™ conductive silver paint (SPI Supplies/Structure Probe Inc., PA, USA) with edges carefully insulated with fast-dry nail enamel (Maybelline, USA). The TiN-buffered substrate was processed in the same way as a comparison.

3. Results and discussion

3.1. Characterizations

Surface morphology of the epitaxially-grown crystalline Fe_3O_4 is shown in Fig. 1, the surface of the 10-nm-thick TiN-buffer layer is flat, smooth, and uniform (Fig. 1A), while the surface of the 140-nm-thick Fe_3O_4 is apparently rougher with island structures composed of epitaxial columnar grains (Fig. 1B) in fairly homogeneous height profiles. These columnar grains evolve from the island nuclei formed from the initially-sputtered Fe_3O_4 layer and coalesce into larger column-like structures with increasing film thickness [18]. These grain-oriented needle-like columnar structures can greatly increase the surface roughness and effective surface area, making it an ideal material for sensing purposes.

Typical XRD profile of the as-synthesized epitaxial Fe_3O_4 on TiN-buffered Si(0 0 1) substrate is displayed in Fig. 2A. A sharp and intense peak at 2θ = 69.1° is attributed to the Si(0 0 4) from the Si(0 0 1) substrate (JCPDS 65-1060). Another comparatively broad peak was observed at 2θ of around 43°. This peak is also observed for the TiN-buffered substrate (data not shown), though not as broad as that for Fe_3O_4 on TiN-buffered substrate, indicating it should be indexed as TiN(0 0 2) at 2θ = 42.6° (JCPDS 65-0715), as reported previously [20]. However, since the lattice parameter of Fe_3O_4 (a = 0.840) is almost twice as that of TiN (a = 0.424), it is quite likely that the peak of Fe_3O_4(0 0 4) at 2θ = 43.1° (JCPDS 65-3107) overlaps with that of TiN(0 0 2), producing a broader peak than that for pure TiN. This result cannot confirm the presence of Fe_3O_4, but can well exclude presence of any other iron oxide species such as FeO and Fe_2O_3 without their signature peaks observed.

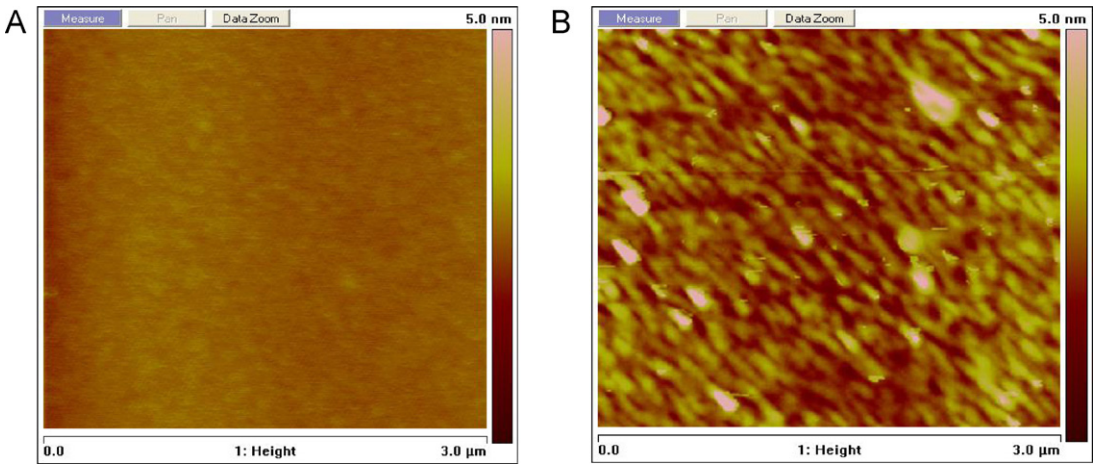

Fig. 1. AFM images of (A) TiN-buffered substrate and (B) Fe_3O_4.

XPS was employed to further confirm the valence state of the synthesized iron oxides. A high resolution spectrum in the Fe 2*p* region is shown in Fig. 2B. Two peaks observed at binding energies of 710.9 and 724.4 eV, are assigned to Fe $2p_{3/2}$ and $2p_{1/2}$ respectively, consistent with published literature [21]. It demonstrates the coexistence of Fe^{3+} and Fe^{2+} valence states from Fe_3O_4 and eliminates possible existence of other iron oxide species also with regards to XRD data. As a result, it can be further confirmed the peaks of TiN and Fe_3O_4 do overlap in XRD profiles, indicating epitaxial Fe_3O_4(0 0 4) was successfully grown on TiN-buffered substrate.

Fe_3O_4 is marked and distinguished from other iron species by its well-known outstanding magnetic properties. Inherent magnetic properties of the epitaxial Fe_3O_4 thin film were investigated by the magnetic hysteresis loops measured by VSM at room temperature (Fig. 2C). The as-synthesized Fe_3O_4 film displayed strong ferrimagnetic behavior with coercivity of about 500 Oe and saturation magnetization greater than 430 emu cc^{-1} which is not even completely saturated in the range investigated, as a typical phenomenon of epitaxially-grown Fe_3O_4 film [22]. The ferromagnetism is reported to be closely associated with anisotropy, arising from the anti-parallel spins with different types and unequal magnitudes of Fe^{2+} and Fe^{3+}cation sites in the interpenetrating sublattices separated by O^{2-} ions [23]. This demonstrates the successful synthesis of Fe_3O_4 with distinct magnetic properties, which may be useful in practical applications.

ATR-FTIR spectra of TiN-buffered substrate and Fe_3O_4 are shown in Fig. 2D. The band at 1108 cm^{-1} is assigned to Si-O-Si while one at 909 cm^{-1} to Si-O-Ti is also present [24]. The band at 580 cm^{-1} in TiN-substrate should be due to vibrations from Ti-N [25], which is observed in Fe_3O_4 to shift to 586 cm^{-1} with decreased intensity possibly due to the interactions and bonding between TiN and initially-sputtered Fe_3O_4. This assumption is supported by a ~2 nm intermixing layer at TiN/Fe_3O_4 interface, with 8% of Ti diffused into Fe_3O_4 [18] as well as the absence of Si-O-Fe bonds around 857 cm^{-1} [26]. The fairly obvious bands, which are only seen in Fe_3O_4 at around 567 cm^{-1} and 666 cm^{-1} are attributed to the Fe-O stretching vibration in octahedral and tetrahedral sites of Fe_3O_4 respectively, in consistent with published data [26,27]. The drastically strong and broad band between 600 and 800 cm^{-1} with the peak centered at round 685 cm^{-1} is considered to be the bending of Fe-O-H, which usually exists in iron oxides [23,28]. These results well support the formation of Fe_3O_4 on the buffer-layer.

To study the electron transfer between the electrolyte and electrode surface, Nyquist complex plane plots were obtained by room-temperature AC-impedance measurements using $Fe(CN)_6^{4-/3-}$ redox probes (Fig. 2E). One semicircle is seen for TiN-buffered substrate, meaning an electron transfer-controlled process with a large electron transfer resistance (R_{ct}) indicated by the diameter of the semicircle. This illustrates the dominance of overall impedance by grain boundary resistance, a typical characteristic of TiN [29]. In Fe_3O_4, however, an entirely different plot is observed, featuring two much smaller consecutive semicircles, which are caused by the competition between dissolution and growth processes on Fe_3O_4 surface. As the equivalent circuit of Fe_3O_4 shows, each parallel RC element is represented by a semicircle with diameters of each more than ten times smaller than that of TiN-buffered substrate, manifesting a much faster electron transfer on the interface and higher conductivity as an electrochemical sensing platform. The dotted lines indicate that the simulated data for each element fit the experimental data well.

3.2. Electrochemical catalytic activity

The electrocatalytic activity of epitaxial Fe_3O_4 sensor towards the reduction of H_2O_2 was investigated by voltammetric responses in CV (Fig. 3). There are no obvious peaks at TiN-modified electrode in the absence of H_2O_2 in the scanned potential range (curve a), while, in contrast, two anodic (at −0.0375 and +0.025 V) and one cathodic peaks can be seen at Fe_3O_4-modified electrode, due to electrochemical behaviors of iron species at different valence states (curve c). The cathodic peak at −0.320 V is probably ascribed to the reduction of Fe(III) in the Fe_3O_4 into Fe, similar to previous observations [30], whereas the anodic peaks are associated with the oxidation of Fe and Fe(II) into Fe(III). With 0.5 mM H_2O_2 added, there is only a minor current response seen for TiN-buffered substrate (curve b), which is negligible compared to the remarkably large increase in reduction current from around 0.0 V occurring at Fe_3O_4-modified electrode (curve d), indicating the Fe_3O_4 thin film is a promising material for sensitive H_2O_2 sensing. The cathodic peak of Fe_3O_4 towards H_2O_2 reduction is around −0.5 V. Fe_3O_4 with valence state of Fe(II) and Fe(III) was therefore identified as the electrocatalyst responsible for H_2O_2 reduction, which proceeds as a two-electron and two-proton participating reduction step with generation of H_2O as products. This sensing process is also accompanied by the reductive valence state of Fe(II) on Fe_3O_4 being oxidized into Fe(III) and after that, oxidative valence state Fe(III) is regenerated back into Fe(II) [31]. Actually, due to the biocompatibility, facile synthesis and ferrimagnetic properties for easy separations, Fe_3O_4 is used as inert support for enzyme immobilization in the detection of H_2O_2 [1]. In our present work, however, the as-synthesized epitaxial Fe_3O_4 is capable of efficiently catalyzing the H_2O_2 reduction itself, making it unsuitable as an inert enzyme

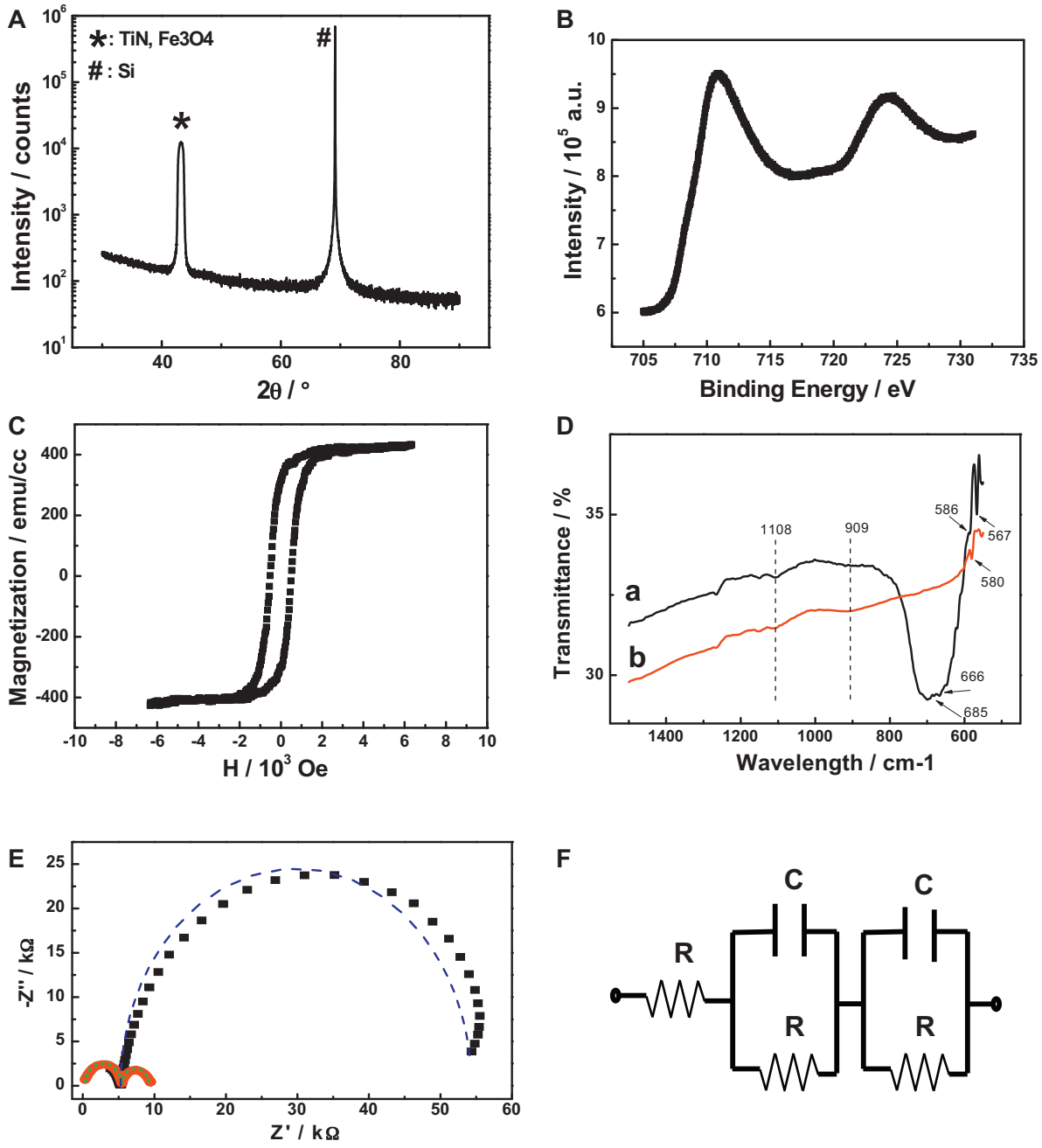

Fig. 2. (A) XRD patterns of Fe_3O_4 on TiN-buffered Si substrate. #Reflections of Si and *the overlapped peaks from Fe_3O_4 and TiN. (B) High resolution XPS spectra of Fe 2*p* region of Fe_3O_4. (C) Magnetic hysteresis loops of Fe_3O_4. (D) ATR-FTIR spectra of TiN-buffered substrate (a) and Fe_3O_4 (b). (E) EIS spectra of TiN-buffered substrate (■) and Fe_3O_4 (•) in 100 mM KCl containing 10 mM $K_4[Fe(CN)_6]/K_3[Fe(CN)_6]$. Dotted lines indicate the simulation results to fit the experimental data, and the inset shows equivalent circuit of Fe_3O_4. R_s: solution resistance, R_{ct}: electron transfer resistance, C_{dl}: double layer capacitance, Z_w: Warburg impedance.

platform but it is appealing as a stable, "green" and inexpensive peroxidase-like material.

3.3. Optimization of sensing

Since the electrochemical catalysis of Fe_3O_4 towards H_2O_2 involves a two-proton process [32], the pH has a strong effect on the sensor performance, predicted to be in favor of mild acidic conditions. The pH dependence of Fe_3O_4-modified electrode was investigated in the pH range of 5.3–8.0 (Fig. 4A). The amperometric response first increased and then decreased with an increase in pH values, reaching the highest current response at pH 5.9, which is chosen as optimal. Unlike the linear increase in current responses with decreasing pH values down to pH 3.0 in a paper on Fe_3O_4 powder [32], there might be an acidic corrosion process undergoing on the thin film surface at too low a pH, and thus decrease its catalytic activity. However, it is worth noting that the amperometric responses do not change much from pH 5.3 to 7.0, with only about 10% difference between the highest and lowest responses, indicating the as-synthesized Fe_3O_4 is highly reliable and stable as a sensor in mild acidic conditions, which is advantageous over the use of enzymes.

The effect of applied potential on the sensor performance was also studied (Fig. 4B). The amperometric response is observed to increase almost linearly with an increase in the applied potential of −0.20 to −0.40 V due to increasing driving force for the electrochemical reduction of H_2O_2 [32] and nearly remains unchanged for applied potential larger than −0.40 V. Regarding many compounds

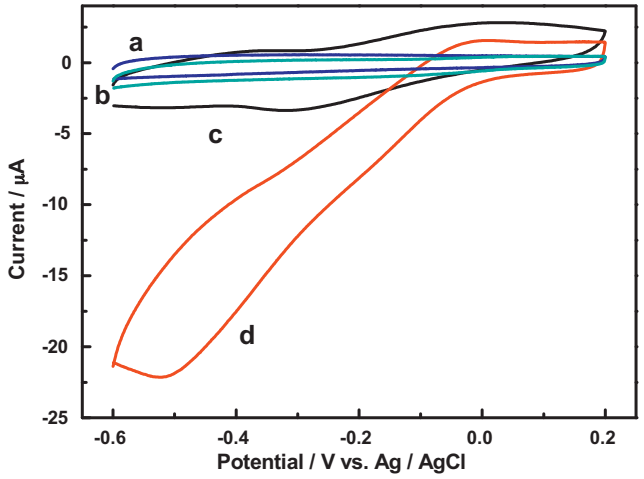

Fig. 3. Cyclic voltammograms of electrodes modified with TiN-buffered substrate (a and b) and Fe_3O_4 (c and d) in pH 5.9 50 mM PBS in the absence (a and c) and presence (b and d) of 0.5 mM H_2O_2. Scan rate: 100 mV s^{-1}.

in real samples and/or reaction intermediates could be electrochemically reactive under high potentials and extreme pH values, it is more appropriate to carry out the detection under mild pH conditions and relatively low potentials. Therefore, −0.4 V was selected as the working potential.

The effect of temperature on the detection was also investigated (Fig. 4C). At temperature ranging from 10 to 50 °C, the amperometric responses against 0.1 mM H_2O_2 is linearly dependent on the temperature, with a slope of −0.082 μA °C^{-1} (R^2 = 0.990), including the ambient condition around 25 °C. Judged by the low increase, the sensor has a fairly stable performance within ±10 °C temperature variance at any temperature in this range. Another linear dependence is observed from 50 to 70 °C, with a slope of −0.627 μA °C^{-1} (R^2 = 0.994). These results suggest the Fe_3O_4-modified electrode has an increasing amperometric response in cathodic current with increase in temperature and at higher temperature, the current response increases more remarkably due to faster electrocatalytic kinetics. An important advantage of this oxide-based non-enzymatic sensor is that it can endure a wider temperature range than enzyme-based sensors. Higher temperature (e.g., 70 °C) results in a higher sensitivity, which allows more sensitive detection of H_2O_2. However, though the sensor exhibits higher catalytic performances at higher temperature, with regards to solution evaporation, convenience, and practical routine uses, our entire study was conducted at room temperature.

The voltammetric behavior at different scan rates of the Fe_3O_4-modified electrode were evaluated (Fig. 5). Identical to Fig. 3 (curve c), two anodic and one cathodic peaks can be observed. With the increasing scan rates from 20 to 200 mV s^{-1}, the two anodic peaks shifted positively while the cathodic peak shifted negatively. Their peak currents all increased linearly (R^2 = 0.988, 0.990 and 0.986 for peaks a1, a2 and c1, respectively) along with the increase in square root of scan rates (Fig. 5 inset). These results reveal a non-surface controlled electrochemical process at Fe_3O_4 electrode, caused by electron hopping. This result was further supported by our finding that the thickness of the thin film (90, 140, 270 nm) does not have any significant influence on the electrocatalytic effect on H_2O_2, in accordance to the non-surface-controlled electrocatalytical process.

3.4. Analytical performances

The amperometric sensing of H_2O_2 at the TiN-substrate and Fe_3O_4-modified electrodes was accomplished at optimal pH 5.9

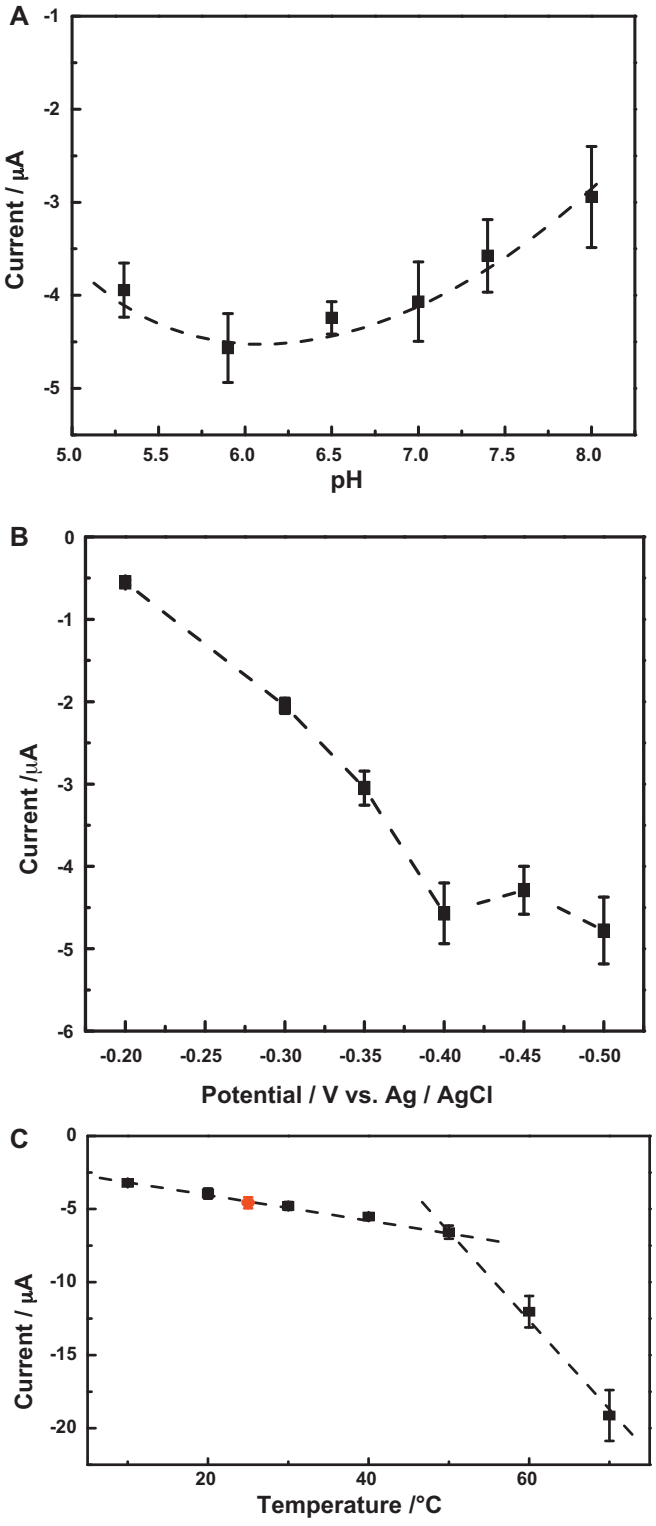

Fig. 4. Amperometric responses of Fe_3O_4 electrode against 0.1 mM H_2O_2 under (A) different pH under at room temperature and applied potential of −0.4 V, (B) different applied potential at room temperature and pH 5.9 of 50 mM PBS, (C) different temperature at pH 5.9 of 50 mM PBS and applied potential of −0.4 V, while (•) indicates measurements at room temperature around 25 °C. Error bars indicate triplicate measurements.

Table 1
Effects of different interferents on H_2O_2 determination by our sensor.

Interferent	Current ratio (%)	Interferent	Current ratio (%)	Interferent	Current ratio (%)
Sucrose	5.60	Glycine	4.55	$Mg(NO_3)_2$	0.85
D-fructose	4.10	Histamine	0.09	$CaCl_2$	4.64
D-(+)-maltose	1.08	Fumaric acid	2.12	$Al_2(SO_4)_3$	0.88
β-D-lactose	0.02	Caffeine	0.10	BSA[a]	3.18
D-(+)-glucose	0.79	Citric acid	3.89	KCl	2.37
Na_2CO_3	0.05	Mannose	2.09	Xanthan gum[a]	0.04
NaCl[c]	1.57	Dopamine	0.06	Ascorbic acid	0.20
Uric acid	0.40	Casein[b]	1.60	β-lactogluboin[a]	5.86
KH_2PO_4[c]	1.86	Na_2HPO_4[c]	2.03		

[a] H_2O_2:interferents = 1:10 (w/w).
[b] H_2O_2:interferents = 1:100 (w/w).
[c] H_2O_2:interferents = 1:100 (molar ratio), all the others: H_2O_2:interferents = 1:1 (molar ratio), due to solubility issues.

and in 50 mM PBS under optimal potential of −0.4 V with stepwise addition of 0.1 mM H_2O_2 (Fig. 6A). Obviously, the amperometric current responses at Fe_3O_4-modified electrode are significantly larger than the nearly negligible responses at TiN-substrate, consistent with the results from CV (Fig. 3b and d), which once again confirms that Fe_3O_4 is the key contributing element in the sensing application. It is also clearly seen that with gradual addition of H_2O_2, the current response first increased and then decreased with further additions, implying a progressive electrocatalytic inactivation in the presence of higher concentration of H_2O_2, possibly caused by the generation of reaction intermediates. A good linear dependence of current response vs. H_2O_2 concentration ($i(\mu A) = -38.9 \times C - 2.34$, $R^2 = 0.991$) at Fe_3O_4 electrode was found within the linear range of up to 0.7 mM (Fig. 6B), with an acceptable sensitivity of 432.2 μA mM^{-1} cm^{-2}. The detection limit is determined to be 1.0 μM (at signal/noise = 3) which is lower than other enzymatic or enzymeless Fe_3O_4-based biosensors such as Fe_3O_4 NP-PDDA composite film [14], HRP-Fe_3O_4-Chitosan modified GCE [1], and Fe_3O_4-Ag hybrid materials [21]. This high sensitivity and low detection limit are owing to the large and rough surface area of epitaxially-grown columnar grains as well as the high electrocatalytic activity of as-synthesized Fe_3O_4.

3.5. Sensor stability and specificity

The stability of the sensor was tested by measuring its current response to H_2O_2 after being stored under ambient conditions and there were no obvious decrease in the response within one week, and lost only about 10% of its original sensitivity over 20 days, suggesting its acceptable stability over this period. The operational stability was also investigated by measuring its amperometric response over 20 min (Fig. 7A), and the current response maintained a stable and well-defined plateau with little observable loss.

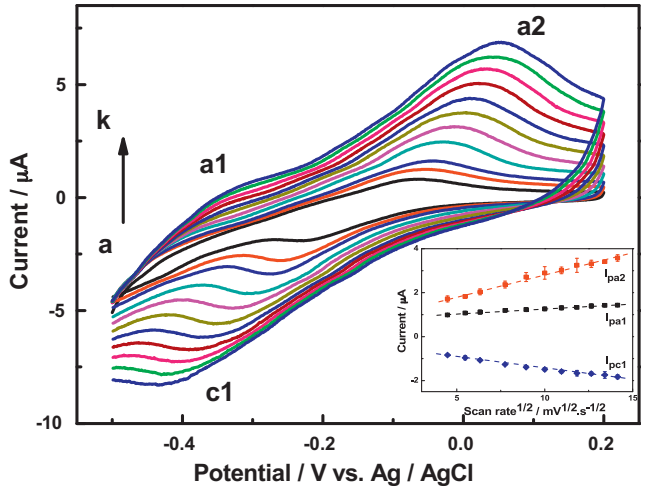

Fig. 5. Cyclic voltammograms of Fe_3O_4 electrode in pH 5.9 in 50 mM PBS at different scan rates of 20, 30, 40, 60, 80, 100, 120, 140, 160, 180 and 200 mV s^{-1} in an increasing order from inner to outer (a–k) as the arrow indicates. Anodic and cathodic peaks are labeled as in the figure. Inset shows the plots of anodic and cathodic peak currents vs. square root of scan rates.

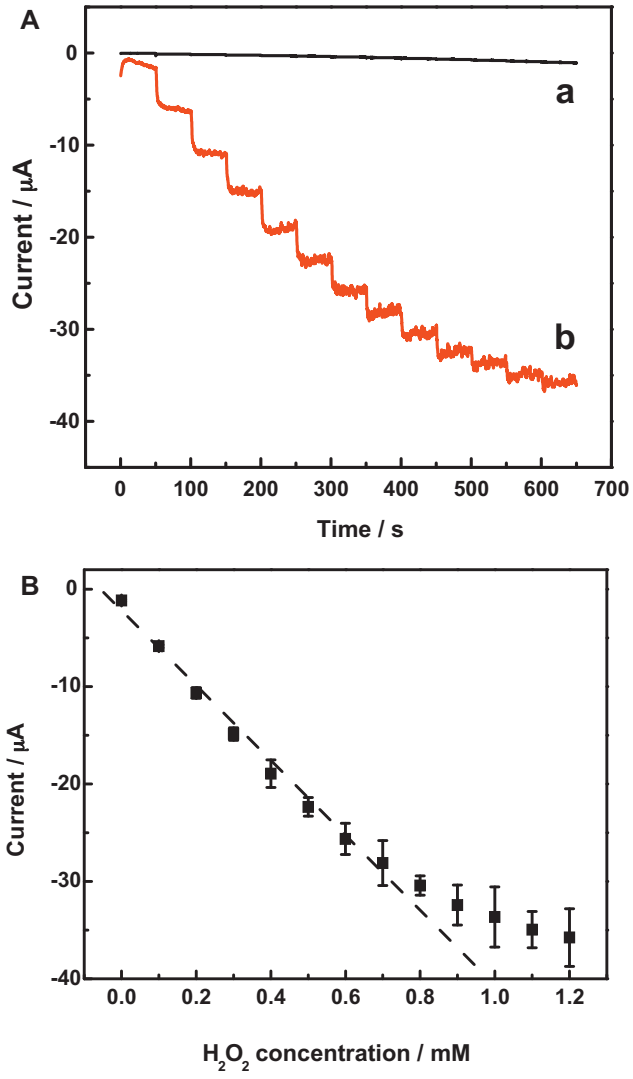

Fig. 6. (A) Current–time responses of (a) TiN-buffered substrate and (b) Fe_3O_4 electrodes with stepwise additions of 0.1 mM H_2O_2 every 50 s. (B) Linear dependence of current response on H_2O_2 concentration at Fe_3O_4 electrode. Error bars indicate triplicate measurements. Applied potential: −0.4 V.

Table 2
Comparing the performance of our sensor to that of an HPLC in determination of H_2O_2 in different commercial samples ($n = 6$).

Samples	HPLC	Our sensor	Recovery rate	Added
Walgreens antiseptic/oral debriding agent	0.736 ± 0.015 M	0.785 ± 0.056 M	99.54%	0.1 mM
Crest whitening mouthwash solution	0.336 ± 0.009 M	0.417 ± 0.034 M	91.74%	0.1 mM
Diet coke	N/A	N/A	101.63%	0.1 mM
Gatorade	N/A	N/A	97.48%	0.1 mM

The sensor responded extremely fast upon addition of H_2O_2 and was able to achieve 95% of steady-state current within about 5 s (Fig. 7A inset). The rapid response could be attributed to the rough surface of the epitaxial thin film as well as the facilitation of electron transfers by the columnar Fe_3O_4 grains. The reproducibility of the sensor was studied by measuring the current response to 0.1 mM H_2O_2 10 times using the same electrode, only with a relative standard deviation of 6.8%. Meanwhile, three electrodes prepared at identical conditions had a RSD of 9.2%. These results confirm satisfactory stability and good reproducibility of our sensor. Given its simple material synthesis, easy preparation and availability for mass manufactures, the epitaxial Fe_3O_4 thin film is a promising material for H_2O_2 sensing.

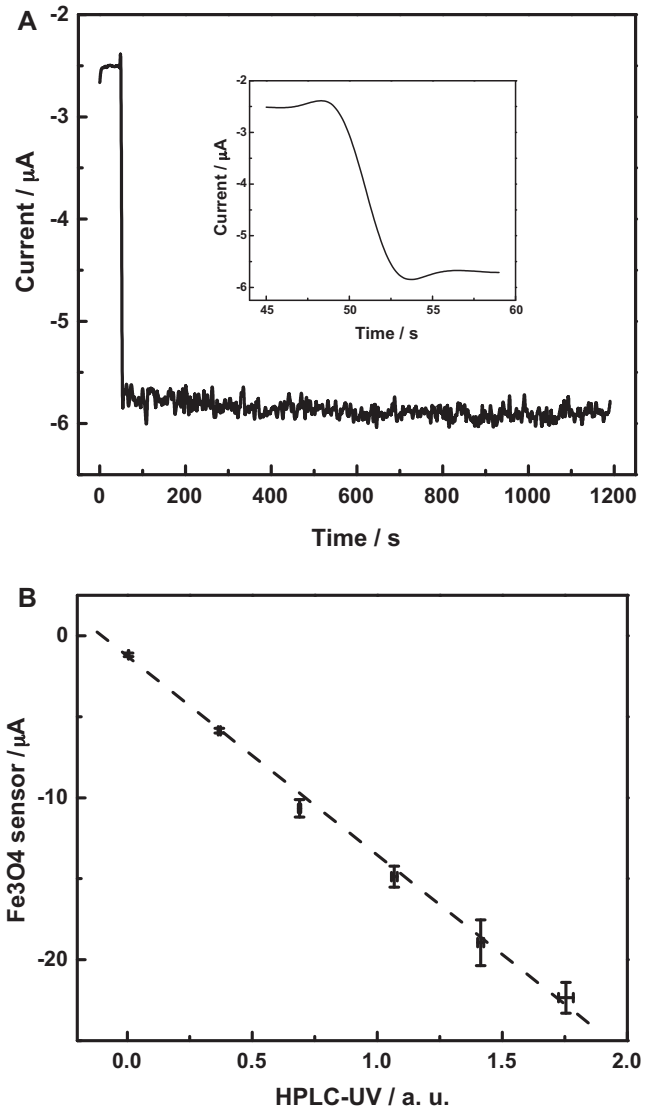

Fig. 7. (A) Stability of the amperometric response of Fe_3O_4 electrode towards 0.1 mM H_2O_2 in pH 5.9 50 mM PBS at −0.4 V over an operational time of 1200 s. Inset shows the response time to achieve a steady-state current. (B) Correlation of Fe_3O_4 sensor to HPLC-UV. Error bars indicate triplicate measurements.

Electrochemically active compounds that can simultaneously generate detectable current signals along with detecting substrates have remained a significant challenge for electrochemical sensors. The general pharmaceutical grade of H_2O_2 for products at drugstores or supermarket such as antimicrobial agents for treating wounds and sanitizing agents is about 3%, while the beautician grade can be 6% for hair coloring. In food industry for production of foods such as cheese, eggs, and whey-containing products, the food grade is as high as 35%. However, though the concentration of H_2O_2 in these real samples is much higher than potentially oxidizable ingredients, it has still been frequently reported that some organic acids such as AA and UA [33,34] as well as some sugars [35] can possibly produce highly influencing electrochemical signals. We examined the specificity of our sensor by investigating a number of interfering species such as sugars, salts, proteins etc. that possibly co-exist with H_2O_2 in real samples. As shown in Table 1, the current response from H_2O_2 sensing was barely influenced by any interferents, producing negligible interferences between 0.02 and 5.86%. Noticeably, high chloride concentration which is usually a major issue for signal loss in most metal or metal oxide based enzymeless sensors, is not observed with our sensor. It could be inferred that our sensor has excellent specificity to H_2O_2 and immune to wide range of interferents and thus is suitable for use as an enzymeless and interference-free sensor in complex sample matrices.

3.6. H_2O_2 testing in real samples

The performance of our sensor was compared with that of a commercially-available HPLC system equipped with UV detector for measuring H_2O_2 in medical and food products. A series of standard H_2O_2 solutions were tested using the two techniques; the results correlated well, with $R^2 = 0.996$ (Fig. 7B). Further tests were conducted using complex matrices which are readily available on the market such as dental care product (Crest Whitening mouthwash solution), sanitizing agent (Walgreens antiseptic/oral debriding agent), and food samples (Diet Coke, Gatorade), which were diluted and tested. The results obtained with our sensor are consistent with those obtained with HPLC-UV (Table 2). Our sensor also displayed acceptable recovery rates and therefore can well serve as a potential candidate for routine analysis both for prevention of internal consumption and monitor in manufacturing and environmental aspects.

4. Conclusions

A facile and easy approach to synthesize epitaxial Fe_3O_4 thin film with needle-like columnar surface structures suitable for mass scale production has been developed. The as-synthesized material displayed extraordinary electrocatalytic activity to H_2O_2 reduction with a dynamic working range of up to 0.7 mM with a low detection limit of 1.0 μM, a rapid response time of less than 5 s and a high sensitivity of 432.2 μA mM^{-1} cm^{-2}. As an ideal enzymeless sensing candidate material, it also has good stability, acceptable reproducibility and satisfying specificity against common interferents co-existing in medical and food products. Taking the

miniaturization of electrochemical devices, it is possible to fabricate a hand-held detection device for routine analysis in industry.

Acknowledgement

We are grateful to Professor Xujun Pan at the University of Wisconsin-Madison for allowing access to HPLC-UV unit in his laboratory.

References

[1] X.C. Tan, J.L. Zhang, S.W. Tan, D.D. Zhao, Z.W. Huang, Y. Mi, Z.Y. Huang, Electroanalysis 21 (2009) 1514.
[2] A. Spector, N.J. Kleiman, R.-R.C. Huang, R.-R. Wang, Exp. Eye Res. 49 (1989) 685.
[3] S. LopezOngil, J.A. GinesRuiz, M.C. Iglesias, P. Ruiz, J. Bujan, D. RodriguezPuyol, Kidney Int. 50 (1996) 1795.
[4] D.B. Humberston, E.P. Krenzelok, J. Toxicol. Clin. Toxicol. 28 (1990) 95.
[5] C.-X. Lei, S.-Q. Hu, G.-L. Shen, R.-Q. Yu, Talanta 59 (2003) 981.
[6] D. Grieshaber, R. MacKenzie, J. Voros, E. Reimhult, Sensors-Basel, 8 (2008) 1400.
[7] P. Yuan, Y. Zhuo, Y. Chai, H. Ju, Electroanalysis 20 (2008) 1839.
[8] C.-L. Hsu, K.-S. Chang, J.-C. Kuo, Food Control 19 (2008) 223.
[9] R. Wilson, A.P.F. Turner, Biosens. Bioelectron. 7 (1992) 165.
[10] X. Li, Q. Zhu, S. Tong, W. Wang, W. Song, Sensors Actuat. B: Chem. 136 (2009) 444.
[11] D. Cao, J. Chao, L. Sun, G. Wang, J. Power Sources 179 (2008) 87.
[12] Y. Tian, Q. Rui, K. Komori, H.Q. Liu, Y.P. Luo, Y. Sakai, Anal. Chim. Acta 670 (2010) 57.
[13] S. Chakraborty, C. Retna Raj, Biosens. Bioelectron. 24 (2009) 3264.
[14] L. Zhang, Y. Zhai, N. Gao, D. Wen, S. Dong, Electrochem. Commun. 10 (2008) 1524.
[15] P. Yu, D. Zhou, Anal. Chim. Acta 300 (1995) 91.
[16] L. Gao, J. Zhuang, L. Nie, J. Zhang, Y. Zhang, N. Gu, T. Wang, J. Feng, D. Yang, S. Perrett, X. Yan, Nat. Nano. 2 (2007) 577.
[17] H. Wei, E. Wang, Anal. Chem. 80 (2008) 2250.
[18] H. Xiang, F.Y. Shi, M.S. Rzchowski, M.S. Voyles, Y.A. Chang, Appl. Phys. Lett. 97 (2010).
[19] H. Xiang, C.X. Ji, J.J. Yang, Y.A. Chang, Appl. Phys. A Mater. 98 (2010) 707.
[20] C.X. Ji, F. Lu, Y.A. Chang, J.J. Yang, M.S. Rzchowski, Appl. Phys. Lett. 92 (2008).
[21] Z. Liu, B. Zhao, Y. Shi, C. Guo, H. Yang, Z. Li, Talanta 81 (2010) 1650.
[22] D.T. Margulies, F.T. Parker, F.E. Spada, R.S. Goldman, J. Li, R. Sinclair, A.E. Berkowitz, Phys. Rev. B 53 (1996) 9175.
[23] S. Zhang, W. Wu, X. Xiao, J. Zhou, F. Ren, C. Jiang, Nanoscale Res. Lett. 6 (2011) 89.
[24] M.Q. Snyder, B.A. McCool, J. DiCarlo, C.P. Tripp, W.J. DeSisto, Thin Solid Films 514 (2006) 97.
[25] A.W. Jackson, O. Shebanova, J. Solid State Chem. 179 (2006), DOI: 10.1016/j.jssc.2006.01.067; PII: S0022-4596(06)00062-4.
[26] S. Thomas, D. Sakthikumar, Y. Yoshida, M.R. Anantharaman, J. Nanopart. Res. 10 (2008) 203.
[27] F.H. Chen, et al., Nanotechnology 19 (2008) 165103.
[28] S. Mitra, et al., Nanotechnology 18 (2007) 275608.
[29] Y. Qiu, L. Gao, J. Phys. Chem. B 109 (2005) 19732.
[30] S.S. Kulkarni, C.D. Lokhande, Mater. Chem. Phys. 82 (2003) 151.
[31] L.M. Rossi, A.D. Quach, Z. Rosenzweig, Anal. Bioanal. Chem. 380 (2004) 606.
[32] M.S. Lin, H.J. Leu, Electroanalalysis 17 (2005) 2068.
[33] L. Xiao, J. Chen, C.-S. Cha, J. Electroanal. Chem. 495 (2000) 27.
[34] X.M. Chen, Z.J. Lin, D.J. Chen, T.T. Jia, Z.M. Cai, X.R. Wang, X. Chen, G.N. Chen, M. Oyama, Biosens. Bioelectron. 25 (2010) 1803.
[35] C. Batchelor-McAuley, Y. Du, G.G. Wildgoose, R.G. Compton, Sensors Actuat. B: Chem. 135 (2008) 230.